BRAIN CONNECTIVITY
Volume 6, Number 6, 2016

DOI: 10.1089/brain.2015.0362

Regional Patterns of Cortical Phase Synchrony in the Resting State

Kaitlyn Casimo,[1] Felix Darvas,[2] Jeremiah Wander,[3] Andrew Ko,[2,4] Thomas J. Grabowski,[5–7] Edward Novotny,[8] Andrew Poliakov,[9] Jeffrey G. Ojemann,[1,2,4] and Kurt E. Weaver[1,5,7]

Abstract

Synchronized phase estimates between oscillating neuronal signals at the macroscale level reflect coordinated activities between neuronal assemblies. Recent electrophysiological evidence suggests the presence of significant spontaneous phase synchrony within the resting state. The purpose of this study was to investigate phase synchrony, including directional interactions, in resting state subdural electrocorticographic recordings to better characterize patterns of regional phase interactions across the lateral cortical surface during the resting state. We estimated spontaneous phase locking value (PLV) as a measure of functional connectivity, and phase slope index (PSI) as a measure of pseudo-causal phase interactions, across a broad range of canonical frequency bands and the modulation of the amplitude envelope of high gamma (amHG), a band that is believed to best reflect the physiological processes giving rise to the functional magnetic resonance imaging BOLD signal. Long-distance interactions had higher PLVs in slower frequencies (≤theta) than in higher ones (≥beta) with amHG behaving more like slow frequencies, and a general trend of increasing frequency band of significant PLVs when moving across the lateral surface along an anterior–posterior axis. Moreover, there was a strong trend of frontal-to-parietal directional phase synchronization, measured by PSI across multiple frequencies. These findings, which are likely indicative of coordinated and structured spontaneous cortical interactions, are important in the study of time scales and directional nature of resting state functional connectivity, and may ultimately contribute to a better understanding of how spontaneous synchrony is linked to variation in regional architecture across the lateral cortical surface.

Key words: functional connectivity; phase flow; phase locking; phase synchrony; resting state

Introduction

The study of spontaneous interactions in the resting state has become a cornerstone of functional imaging research. Mean correlations of endogenous BOLD signal interactions in the 0.01 Hz range reflect to a good degree the brain's intrinsic functional architecture (Biswal et al., 2010; Damoiseaux et al., 2006), and frequently mimic patterns of task-based functional magnetic resonance imaging (fMRI) responses that support an array of complex cognitive functions (Smith et al., 2009). While resting state fMRI studies have substantially contributed to our understanding of the brain's intrinsic and dynamic functional connectivity, the electrophysiological interactions that define resting state at a systems level are still far less understood (Cabral et al., 2014).

Correlation between resting state fMRI (rsfMRI) and electrophysiological recordings has been well characterized in the slow frequencies accessible with fMRI (<1 Hz), especially with simultaneous electroencephalography (EEG)-fMRI. While the full range of regional band-limited power estimates has been shown to correlate with the spatial distribution of rsfMRI functional networks (e.g., Conner et al.,

[1]Graduate Program in Neuroscience, University of Washington, Seattle, Washington.
Departments of [2]Neurological Surgery and [3]Bioengineering, University of Washington, Seattle, Washington.
[4]Department of Neurosurgery, Harborview Medical Center, UW Medicine, Seattle, Washington.
Departments of [5]Radiology and [6]Neurology, University of Washington, Seattle, Washington.
[7]Integrated Brain Imaging Center, UW Radiology, Seattle, Washington.
[8]Department of Neurology, Center for Integrated Brain Research, Seattle Children's Hospital, Seattle, Washington.
[9]Department of Radiology, Center for Clinical and Translational Research, Seattle Children's Hospital, Seattle, Washington.

2011; Hiltunen et al., 2014; Mantini et al., 2007; Schölvinck et al., 2013), subdural recordings have shown that <1 Hz electrophysiological fluctuations within the amplitude envelope of high frequency oscillations better reflect physiological processes related to the generation of resting state BOLD interactions (Keller et al., 2013; Ko et al., 2011, 2013; Nir et al., 2008).

We investigated oscillations across the full range of band-limited frequencies, including the high gamma (HG; 70–200 Hz) band and low-frequency modulations of the HG amplitude. The contribution of this full broadband range to our understanding of resting state functional connectivity has not been previously reported. This is in part due to the greater susceptibility of EEG and magnetoencephalography (MEG) surface recordings to biological noise of noncortical origin and volume conduction effects due to their distal recording position. The combined effect reduces spatial and amplitude resolution, particularly within the HG band (Buzsáki et al., 2004). Alternatively, electrocorticographic (ECoG) recordings, in which electrodes are placed directly on the human cortical surface, enables high fidelity sampling of high frequencies such as HG with high spatial and temporal precision, though the recording area is limited spatially (Olson et al., 2016). This access to the HG band is particularly important given its postulated role as a marker of evoked local activity (Crone et al., 2006; Miller et al., 2009). Further, ECoG potentials are only minimally impacted by cardiorespiratory artifacts (Kern et al., 2013), a critical factor for studies of slow and infraslow bands that overlap within the same frequency range (Deckers et al., 2006).

Coordinated phase relationships are thought to represent the synchronization of large populations of neurons across and between local and distant sites (Darvas et al., 2009b; Hillebrand et al., 2012; Sauseng and Klimesch, 2008). Such coordination is postulated to represent a mechanism of information transfer, driving influence from one region to another, or synchronizing spatially separated regions of a network (Tognoli and Kelso, 2009). In the resting state, such connectivity encompasses a broad array of connections across the cortex, some of which form organized, intrinsic resting state networks (Biswal et al., 2010; Weaver et al., 2016). Here, we focus on anatomical variation in resting state functional connectivity across the whole cortex, rather than a specific network.

Most electrophysiological studies to date have characterized phase synchrony in event-related, behavioral settings (Lachaux et al., 1999; Sauseng and Klimesch, 2008); few studies have investigated phase interactions in resting state, particularly those in the HG range. Hillebrand et al. (2012) found frequency-dependent spatial variation in phase coherence, but did not examine directional effects. In contrast to more commonly used correlation and coherence measures, such phase-based approaches of functional connectivity are minimally impacted variations in amplitude, and allow inference of directionality and thus causal relationships (Hillebrand et al., 2012; Lachaux et al., 1999; Nolte et al., 2008).

We examined a wide range of canonical band-limited frequency ranges. The amplitude modulation of the high gamma (amHG) band correspond to the time scales observed in BOLD rsfMRIFC, and correlate with observed general network distribution of rsfMRI functional connectivity (FC) studies (Keller et al., 2013; Ko et al., 2013). Here, we examine the slow (0.1–1 Hz) range of amHG. It has been proposed that the amHG band may reflect long-range patterns of connectivity and overlapping neural processes that generate spontaneous BOLD signals, providing a link between electrophysiology and well-documented rsfMRI connectivity (e.g., Gohel and Biswal, 2015; He et al., 2008; Keller et al., 2013, 2014; Ko et al., 2011, 2013). While one focus of this study is phase interactions within the slow amHG band, connectivity across more canonical frequency bands are consistent when measured by stable patterns of high pairwise correlation (Kramer et al., 2011). Therefore, we investigated properties of phase synchrony to assess band-limited functional connectivity (Greenblatt et al., 2012) across the broad neurophysiological spectrum.

Prior work on resting state functional state connectivity (e.g., Kramer et al., 2011) found network patterns that were specific to different frequency ranges. Typically, there was a higher degree of spatial variability in higher frequencies (i.e., ≥beta), and more consistent patterns at lower frequencies (see also Sauseng and Klimesch, 2008; Groppe et al., 2013). Causal relationships have also been explored to a limited extent (Sauseng and Klimesch, 2008), but overall, electrophysiological characteristics of resting networks are still poorly understood.

We employed the phase locking value (PLV; Lachaux et al., 1999), and for directional (pseudo-causal) relationships, the phase slope index (PSI; Nolte et al., 2008). PLV measures the consistency in phase difference between two linear oscillators, while PSI is a measure of pseudo-causal interaction between two signals based on a consistent phase lag across frequencies (Nolte et al., 2008). We used PSI as an alternative to other causality estimates because it is straightforward to interpret and nonparametric, unlike Granger causality, though it does not estimate flows in each direction separately and its estimates are pseudo-causal rather than causal in the Granger sense (Greenblatt et al., 2012).

The goal of this study was twofold: (1) evaluate regional cortical phase relationships in resting state electrophysiology in subdural recordings, with specific focus on variation across frequency bands and anatomical regions; and (2) to test for the presence of directional interactions. Our subdural measurements are highly spatially specific and minimally impacted by volume conduction effects. We find that the dominant frequency of phase interactions increases as a function of anterior-posterior position along the lateral surface of the cortex. We also observed frontal-parietal directional connectivity across a wide range of frequencies. These effects may reflect the unique contributions of each region to the overall organization of spontaneous phase interaction within the resting state.

Materials and Methods

Subjects

Eight patients (5 female, age range 10–42) with intractable epilepsy were recruited from the surgical programs at Harborview Medical Center (HMC, $n=5$) Regional Epilepsy Center and Seattle Children's Hospital (SCH). Each subject had only left ($n=6$) or right ($n=2$) hemisphere electrodes (Fig. 1). All patients were hospitalized for long-term electrophysiological monitoring with implanted ECoG electrodes as part of surgical treatment. Placements of ECoG arrays were

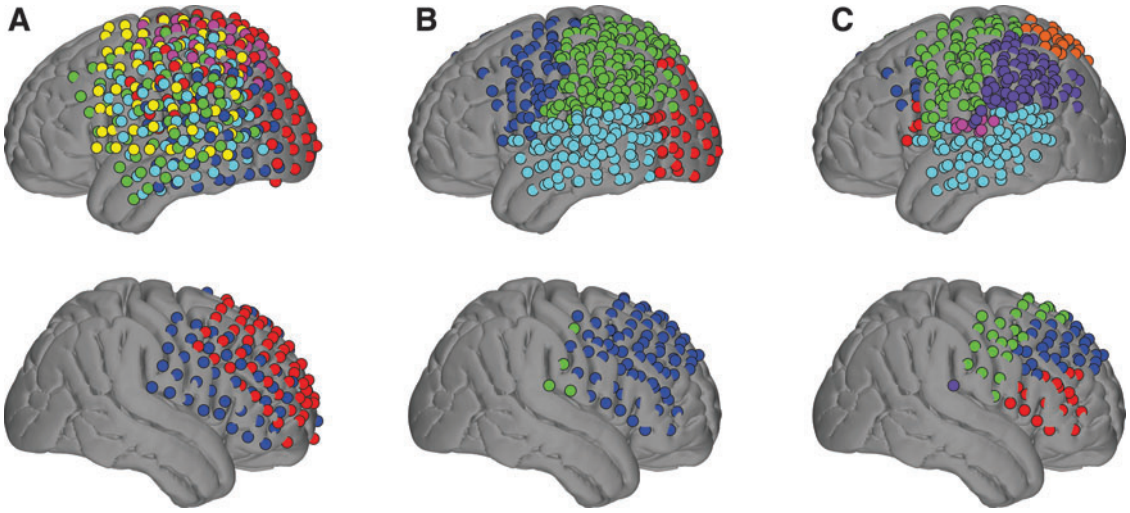

FIG. 1. All electrode placements for all subjects (8 subjects, 480 electrodes). Interhemispheric and occipital lobe electrodes were excluded from analysis due to insufficient sample size. **(A)** Color coded by subject. **(B)** Color coded by lobe. **(C)** Color coded by anatomical ROI. (Blue: dlPFC, BA 8, 9, 46. Red: inferior PFC, BA 44–47. Green: sensorimotor, BA 1–6. Light blue: inferior temporal, BA 20–22. Pink: superior temporal, BA 41–42. Purple: lateral parietal, BA 39–40. Orange: superior parietal, BA 7. BA, Brodmann area; dlPFC, dorsolateral prefrontal cortex; PFC, prefrontal cortex. Color images available online at www.liebertpub.com/brain

determined by clinical needs. All recordings were obtained with subdural platinum ECoG arrays (Ad-Tech, Racine, WI or Integra Lifesciences, Plainsboro, NJ; electrode surface diameter 2.3 mm, 1 cm inter-electrode spacing). All patients provided informed consent in accordance with University of Washington and Seattle Children's Hospital Institutional Review Boards.

Data acquisition

MRIs were acquired preoperatively at HMC on a Phillips 3T Achieva and at SCH on a Siemens 3T Magnetom MRI scanner, both with an 8-channel SENSE head coil. For all patients, an MPRAGE high-resolution T1 sequence (echo time 6.5 msec, repetition time 3 msec, flip angle 8°, matrix size 265×265, 170 sagitally aligned 1 mm slices) was acquired for anatomical volume registration and surface reconstructions.

ECoG recordings were obtained postoperatively at the patient's bedside. The patient was instructed to remain awake, silent, and still during an 8-min block. Patients were verbally reminded to stay awake if they appeared to be falling asleep. Guger g.USBamps (GugerTech, Graz, Austria) amplifiers were used for all recordings. Recordings were controlled using BCI2000 software (Schalk et al., 2004). Data were recorded with DC coupling and with a hardware-imposed notch filter at 60 Hz to remove line noise and low-pass filtered at 500 Hz. A standard scalp reference electrode was used for HMC patients and a subgaleal reference for SCH patients (Olsen et al., 2016).

Analysis

Anatomical labeling. ECoG electrode positions were rendered and labeled as previously detailed (Blakely et al., 2009). Electrode positions were identified on a high-resolution postoperative CT scan using BioImage Suite (Papademetris et al.). The CT scan for each subject was then co-registered to native preoperative 1 mm isotropic MPRAGE using an affine registration. The transformation matrix was applied to all electrode position coordinates. A secondary transform warped the native MPRAGE and native electrode positions into 1 mm MNI brain space. MNI coordinates were transformed to Talairach space using the MNI anatomical labeling atlas, and Brodmann area (BA) labels were estimated using the Talairach Daemon Client (Talairach and Tournoux, 1988). For visualization, electrodes were placed on the MNI cortical surface. Surface renderings were generated by segmenting the MNI volume using FreeSurfer image analysis suite (freely available to download at http://surfer.nmr.mgh.harvard.edu/) and MATLAB. Center coordinates from each electrode at the group level were projected onto surface rendering, and electrodes separated by individual subject (Fig. 1A), lobe (Fig. 1B—frontal, temporal, parietal), or Talairach functional anatomical labels (Fig. 1C—frontal: dorsolateral prefrontal cortex [dlPFC], inferior frontal, sensorimotor; temporal: inferior temporal, superior temporal; parietal: lateral parietal, superior parietal).

Preprocessing. All data processing and analysis were performed in MATLAB (MathWorks, Natick, MA). Preprocessing included manual removal of nonphysiological artifacts, interictal activity, or excessive noise. A common average reference across the ECoG grid was used to reject common mode noise.

Signals were band-pass filtered for each frequency band of interest (delta, 0–4 Hz; theta, 4–8 Hz; alpha, 8–12 Hz; beta, 12–18 Hz; HG, 70–200 Hz) using a zero-phase shift, fourth order Butterworth filter. Instantaneous phase and amplitude estimates across all channels for each frequency band were calculated using the Hilbert transform.

For the HG band only, amplitude modulation (amHG) was also calculated. Estimates were computed according to previously published methods (Keller et al., 2013; Ko et al., 2013) and consisted of a secondary, fourth order Butterworth filter applied to the HG amplitude envelope. Amplitude modulation

was calculated for only the HG band in light of previous results suggesting that slow amHG oscillations uniquely represent resting state network properties (Ko et al., 2011, 2013).

Power spectra for each electrode across the full resting state time series were estimated using a fast Fourier Transform (FFT) averaged across 2 sec of tapered Hanning windows. We sorted the electrodes according to two anatomical distinctions: (l) lobe (Fig. 1B) and (2) cytoarchitecture regions of interest (Fig. 1C). We then averaged the power spectra for all electrodes in each region (Fig. 2A).

Connectivity measures. Pairwise connectivity between electrodes for each individual subject was evaluated with the PLV and the PSI. Both measures were calculated for all frequency bands of interest between all channel pairs for each subject, then pooled between subjects. Mean PLV was calculated across the full time series using the formula introduced in Lachaux et al. (1999), $PLV = \Sigma e^{i*\Delta\theta}$ where $\Delta\theta$ is the instantaneous difference in phase between the two signals. It provides a measure of the consistency in phase difference between two signals for the full resting state period.

PSI was calculated using the formula introduced in Nolte et al. (2008), $PS = \Im(\Sigma_{f\in F} C^*_{ij}(f) C_{ij}(f+\delta f))$, where $\Im$ is the imaginary part, C is the complex coherency, and f is each frequency to a maximum of F. It is a pseudo-causal measure of lag between two signals, indicating the consistency of the direction of lag, which Nolte et al. (2008) define as the primary direction of information transfer. A positive PSI between signals A and B reflects an overall greater influence of signal A on signal B, but does not exclude a lesser influence of signal B on signal A. PSI is an asymmetric measure: for a pair of signals, one will be assigned a positive value denoting pseudo-causal effect, while the other will be assigned the negative of that value denoting being caused. The mean PSI of a region will therefore be positive if the signals from that region provide more than they receive information. Since PSI is calculated using a sliding window over the full time series, and too few delta cycles were included in the window for statistical significance to be established using the phase shuffling procedure, this band was excluded from PSI analysis.

Statistical analysis. We corrected for multiple comparisons and established statistical significance thresholds for both the PLV and PSI interaction metrics using a nonparametric maximum value permutation test (Bullmore et al., 1999). Surrogate data were generated by randomly shuffling the phase component of the broadband signal, extracting frequency bands, and recalculating PLV and PSI as above. Each iteration of this permutation procedure produced $(n \times n)/2 - n$ interactions, where n is the number of electrodes (ranging from 48–64 per subject, yielding 1152–2048 surrogate interactions, respectively). To generate a null distribution of no significant phase interaction, we retained the resulting 50 highest values and then repeated the process 20 times. This

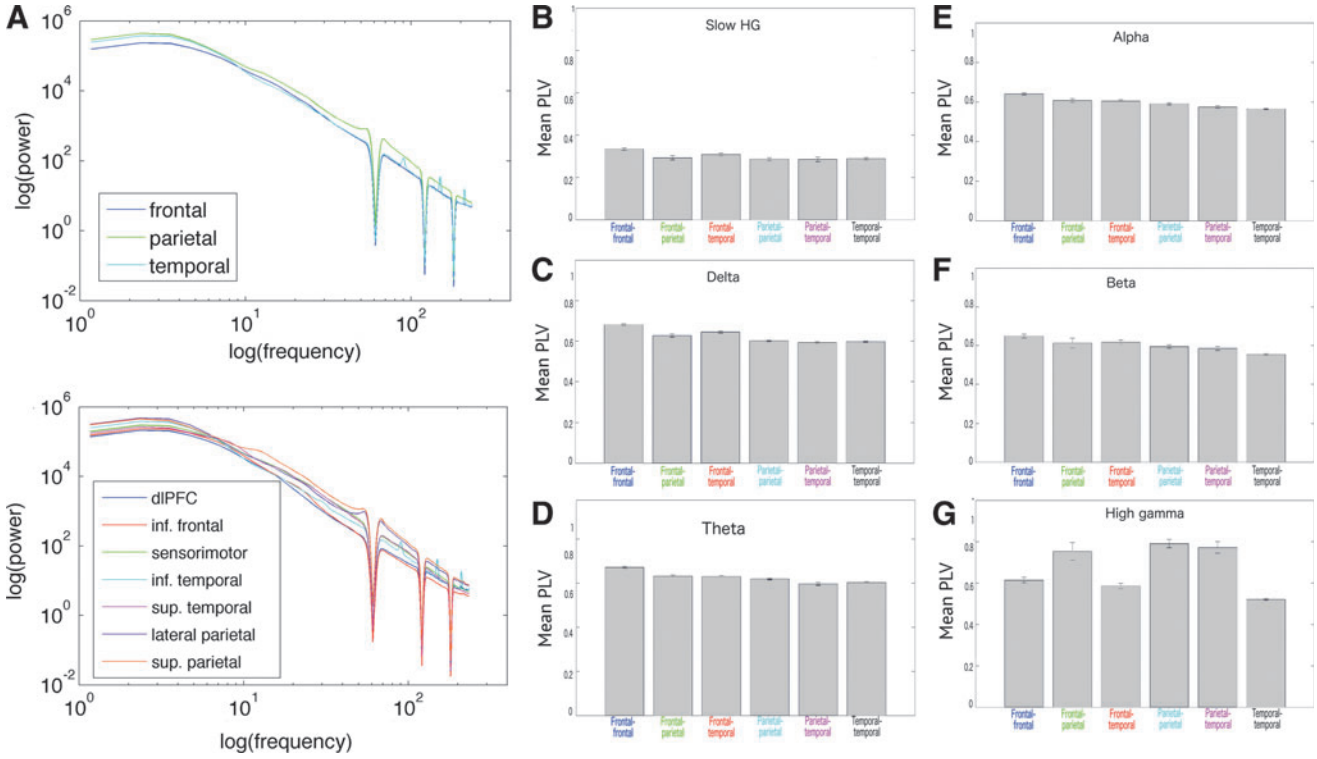

FIG. 2. Power spectra for all subjects by lobe **(A**, top) and by functional anatomical region **(A**, bottom). The spatial distribution of spectra is consistent with prior studies (c.f. Groppe et al., 2013). Mean lobe-to-lobe PLV for **(B)** 0.1–1 Hz slow amHG oscillations, **(C)** delta (0–4 Hz), **(D)** theta (4–8 Hz), **(E)** alpha (8–12 Hz), **(F)** beta (12–18 Hz), **(G)** high gamma (70–200 Hz). Intra-frontal PLVs are consistently higher than intra-parietal or parietal-temporal PLVs across alpha and slower (including amHG) frequencies, while both intra-frontal and intra-parietal connectivity is significantly lower than other pairs' PLVs in HG. amHG, amplitude modulation of high gamma; PLV, phase locking value. Color images available online at www.liebertpub.com/brain

approach produced a distribution of 1000 repetitions and served as basis for statistical comparison. Since we retain the maximum values across all channel pairs under the null hypothesis, this approach minimizes the impact of artificially low estimates stemming random selection (i.e., selecting low synchrony estimates arising from, e.g., large cortical distances between coupling electrodes).

The 95th percentile of the empirical null distribution created with this procedure was set as the threshold for statistical significance (i.e., alpha level $p < 0.05$ chance under the null hypothesis of random phase interactions). Values above this threshold were considered statistically significant and retained for further analysis, and values below were discarded. The total number of electrodes varied substantially between regions, as did the number of subjects contributing electrodes (Table 2A). This was due to the variation in clinical needs and placement of electrodes for individual patients. Importantly, only statistically significant comparisons were included in analysis. In addition, mean PLV or PSI values at the group level for any lobe or BA functional region were discarded if a regional contrast did not have at least two subjects contribute electrodes (Table 2A, B). Statistical significance in mean phase interactions across functional boundaries were evaluated using a one-way analysis of variance (ANOVA), investigating significant individual contrasts using Tukey–Kramer *post hoc* tests.

Results

Electrode location

Electrode locations varied between patients, but were generally located in the lateral portions of the parietal, posterior frontal, and temporal regions (Tables 1 and 2 and Fig. 1). The grid extended partially into the occipital lobe in one subject (<12 channels), and two subjects had interhemispheric electrode strips (both 1×8). However, due to the limited number of samples from these regions, these electrodes were excluded from analysis. Additionally, only four of eight subjects had electrodes in the superior parietal regions, two of which had two and three electrodes, substantially limiting the number of possible pairs involving this region (Fig. 1A). All further analysis considers statistically significant pairwise analyses, drawn from an initial pool of 480 electrodes. We observed regional spatial patterns of resting power spectra consistent with previous studies (Fig. 2A; Duff et al., 2008; Groppe et al., 2013).

Table 1. Subject Demographics, Electrode Placement, and Number of Electrodes

Age	*Gender*	*Grid location (No. of electrodes)*
11	F	L temporal (48)
13	F	L frontal (64)
13	M	L temporal (64)
20	M	L temporal/parietal (64)
35	F	L temporal (64)
37	F	L frontal/temporal (64)
37	M	R frontal, interhemispheric (64)
42	F	R frontal, interhemispheric (64)

Table 2. Electrode Location by Functional Region

dIPFC	*Inf. frontal*	*Sensorimotor*	*Inf. temporal*	*Sup. temporal*	*Inf. parietal*	*Sup. parietal*
(A)						
5	4	8	4	5	7	4
(B)						
0	0	3	9	9	12	0
0	0	17	0	0	12	7
2	0	16	14	10	15	0
0	0	13	0	2	14	12
1	5	24	5	11	14	3
6	1	15	9	12	15	0
22	12	21	0	0	1	2
31	5	14	0	0	0	0

A: Number of subjects contributing electrodes to each functional region. B: Number of electrodes contributed by each subject to each region. Subjects are in same order as Table 1.

Nondirectional connectivity between lobes

Connectivity within and across lobes. Average PLVs across channel pairs varied significantly across both lobe pairs and frequency bands, though absolute variation was small. The mean PLV of the amHG band (Fig. 2B) across all lobe pairs was much lower than mean PLV in other frequency bands (Fig. 2C–G). This may reflect the lower total number of cycles available for computing synchrony in this range compared to other canonical bands. Despite the relatively low PLV estimates in the amHG band, the pattern of increased frontal-frontal and frontal-temporal PLV is comparable to the other slow frequency bands (e.g., delta/theta, Fig. 2B–D). Notably, mean amHG PLV was significantly higher within the frontal lobe than between temporal and parietal lobes and within the parietal lobe; while these differences were small, they were statistically significant (one-way ANOVA, Tukey–Kramer *post hoc* tests, $p < 0.001$).

We observed little absolute difference between delta, theta, alpha, and beta in the distributions of mean PLV between lobes (Fig. 2C–F), but as above, these differences were statistically significant. In these bands, the intra-frontal mean PLV is consistently higher, and intra-parietal PLV lower, than any other intra- or inter-lobe relationship, with the difference in mean inter-lobe PLV decreasing as frequency increases (one-way ANOVA, Tukey–Kramer *post hoc* tests, $p < 0.001$). In contrast, in the HG band, intra-frontal mean PLVs were lower than all relationships except frontal-parietal and intra-parietal mean PLVs (one-way ANOVA, Tukey–Kramer *post hoc* tests, $p < 0.001$) (Fig. 2G).

Connectivity over distance. We examined PLV as a function of distance between each electrode pair (Fig. 3). PLV was lower between more distant electrodes irrespective of frequency, and there were fewer phase relationships between widely spaced sites. Generally, more distant electrode pairs showed significant PLV only in slower frequencies (≤alpha), while nearer neighbor electrode pairs had significant PLV in a much wider range of frequencies. The highest PLVs, indicating very consistent resting state phase relationships, were overwhelmingly nearest neighbor electrodes (inter-electrode distance ≤10 mm) located within

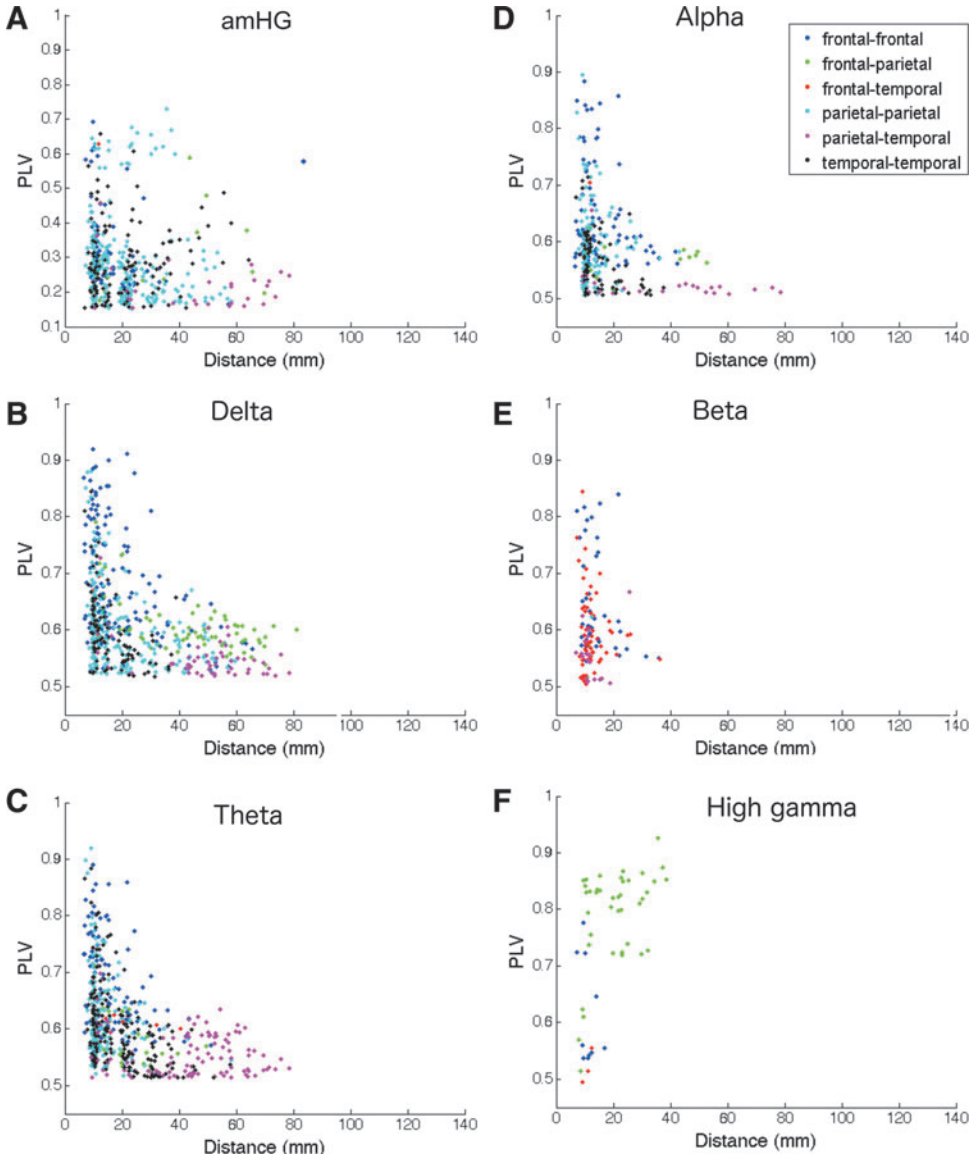

FIG. 3. **(A–F)** PLV as a function of distance between electrode pairs, color-coded by lobe pair. Inter-electrode spacing is 10 mm. **(A)** 0.1–1 Hz slow amHG oscillations, **(B)** delta (0–4 Hz), **(C)** theta (4–8 Hz), **(D)** alpha (8–12 Hz), **(E)** beta (12–18 Hz), **(F)** high gamma (70–200 Hz). Colors: blue, frontal-frontal. Green: frontal-parietal. Red: frontal-temporal. Light blue: parietal-parietal. Pink: parietal-temporal. Black: Temporal-temporal. Note, vertical scale of **(A)** is different from all others. **(G)** Mean distance between pairs of electrodes with significant PLV as a function of frequency band. Unsurprisingly, the highest PLVs were typically found between nearest neighbor electrodes, and long-range connectivity was found almost exclusively in slow (≤alpha, including amHG) frequencies. Color images available online at www.liebertpub.com/brain

the same lobe. Distant parietal-temporal pairs in particular exhibited a narrower range of low PLVs relative to other lobe pair relationships (Fig. 3, pink markers); in contrast, frontal-parietal pairs had somewhat higher PLVs, and shorter inter-electrode distance, than parietal-temporal pairs (Fig. 3, green markers).

Due to its proximity to cortex, ECoG is less affected by volume conduction than noninvasive methods are, but we cannot exclude potential effects on linear measures of synchrony. Low frequency oscillations (≤alpha) in particular, known to spread over large areas (Groppe et al., 2013), can cause spuriously high synchrony measures due to the influence of a distant generator that impacts multiple sites. Synchrony values, measured with PLV, will be a mixture of true synchrony and volume conduction.

Our permutation test does not account for this type of spurious synchrony, as our resampling methods destroy any linear correlations between signals and thus do not preserve volume conduction effects. If there were substantial volume conduction, we would expect significant PLV for all electrode pairs in a band, and that nearby sources will always appear more synchronized than distant ones. However, importantly, most electrode pairs did not exhibit significant synchronization as measured by this test, and particularly for HG did not follow the distance-PLV relationship predicted by volume conduction. We conclude that the effects observed are more likely to come from true neural synchrony rather than primarily from volume conduction.

Nondirectional connectivity between functional anatomical regions

We examined mean PLV between functional anatomical regions (Fig. 1C). The lower PLVs seen in the amHG band relative to all other bands were again evident (Fig. 4A). Again, regions near each other (along diagonal in plots of Fig. 4) had generally higher PLVs than more distant regions (near corners). For the reasons discussed above, this is more

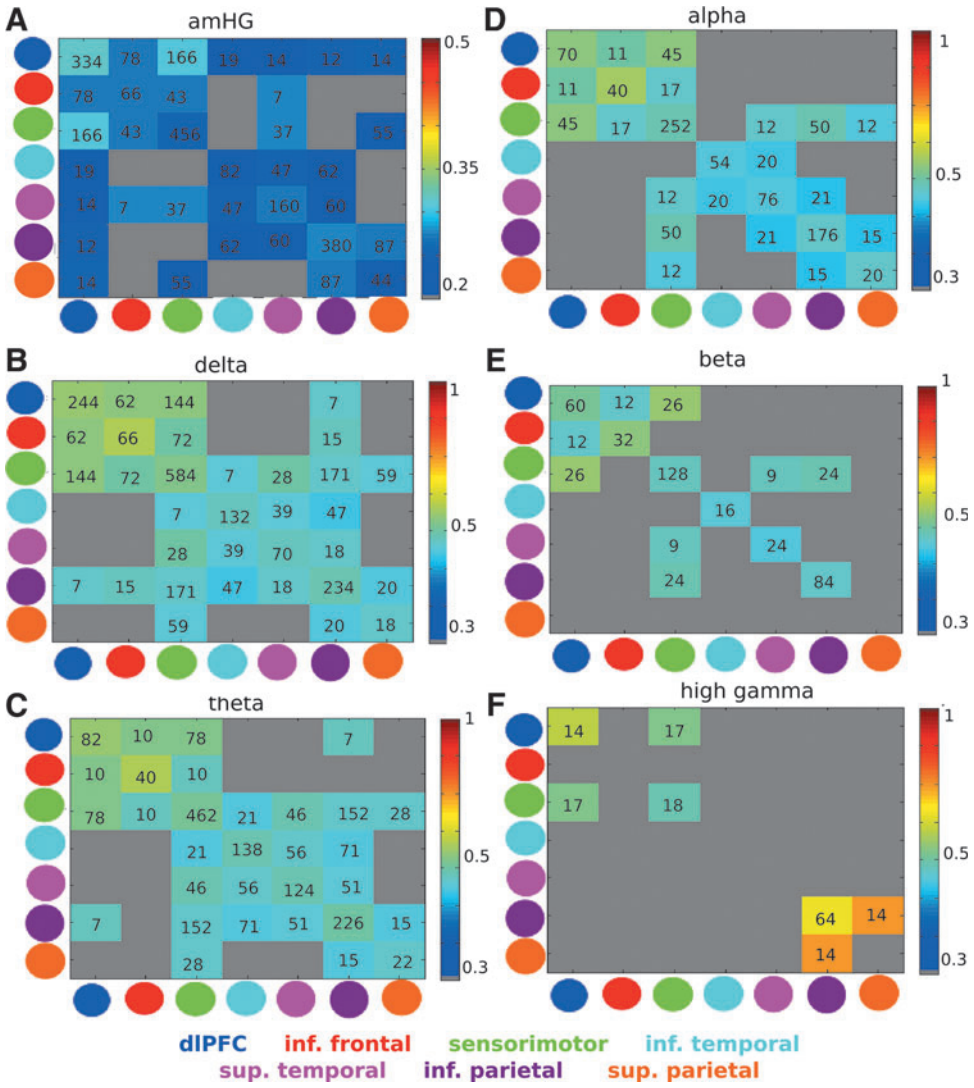

FIG. 4. Mean region-to-region PLV for **(A)** 0.1–1 Hz slow amHG oscillations, **(B)** delta (0–4 Hz), **(C)** theta (4–8 Hz), **(D)** alpha (8–12 Hz), **(E)** beta (12–18 Hz), **(F)** high gamma (70–200 Hz). Along the axes of the connectivity matrix, functional anatomical regions are ordered roughly anterior to posterior. Value in each box indicates number of pairs included in each comparison; comparisons with fewer than seven pairs were excluded. Gray indicates pairs of regions with no significant interactions. We observed an increase in dominant frequency with significant PLV along an anterior-to-posterior gradient, such that significant HG interactions **(F)** were found more in parietal regions, while amHG interactions were more prevalent in frontal regions **(A)**. Color images available online at www.liebertpub.com/brain

likely reflective of true synchrony and not volume conduction. Electrode grid size is limited to 7–8 cm. Due in part to the prevalence of the sensorimotor cortex as a clinical target for grid placement, coverage of the anterior frontal and superior parietal sites was limited relative to other regions. Thus, there are few opportunities to observe connectivity between very distant sites.

Overall, we observed a gradient of preferred PLV frequency across a lateral anterior-to-posterior cortical surface. Specifically, in lower (≤alpha) frequency ranges, mean PLVs were higher in the anterior relative to the posterior regional pairs (Fig. 4A–D). Conversely, in higher (≥beta) frequency ranges, mean PLVs were higher in posterior relative to anterior pairs (Fig. 4E–F). Consistent with the results of PLV over distance, resting state HG connectivity overwhelmingly serves nearest neighbor regions (Fig. 4F). As noted above (Figs. 2 and 3), generally speaking, lower frequencies are more dominant relative to higher frequencies in long-range connections and over a wider range of anatomical areas. Given this, low frequencies have higher frontal/temporal synchrony, and high frequencies have higher PLV temporal/parietal synchrony. Unfortunately, the small number of sampling electrodes in the superior parietal region, dlPFC, and inferior frontal regions also limits our interpretations.

Directional connectivity between functional anatomical regions

Although Figure 4 clearly illustrates the trend of the dominant phase locking relationship shifting to higher frequencies while moving along the lateral posterior surface, it does not indicate a causal or temporal order of these relationships. We used PSI, a pseudocausal measure of connectivity. Net flow as measured by PSI (Nolte et al., 2008) is a metric of the overall direction of information transfer between signals, and it is applied in this context here for the first time.

We focused on PSI between functional anatomical regions (Fig. 5). Due to the limitations outlined in the methods, we excluded the delta band. Generally, PSIs are consistent with PLVs, including PSIs being higher in ≤alpha frequencies (Figs. 4B–D and 5A, B), and PSIs within a lobe (directional flow from one part of a single lobe to another) being typically higher than between two different lobes (Fig. 5).

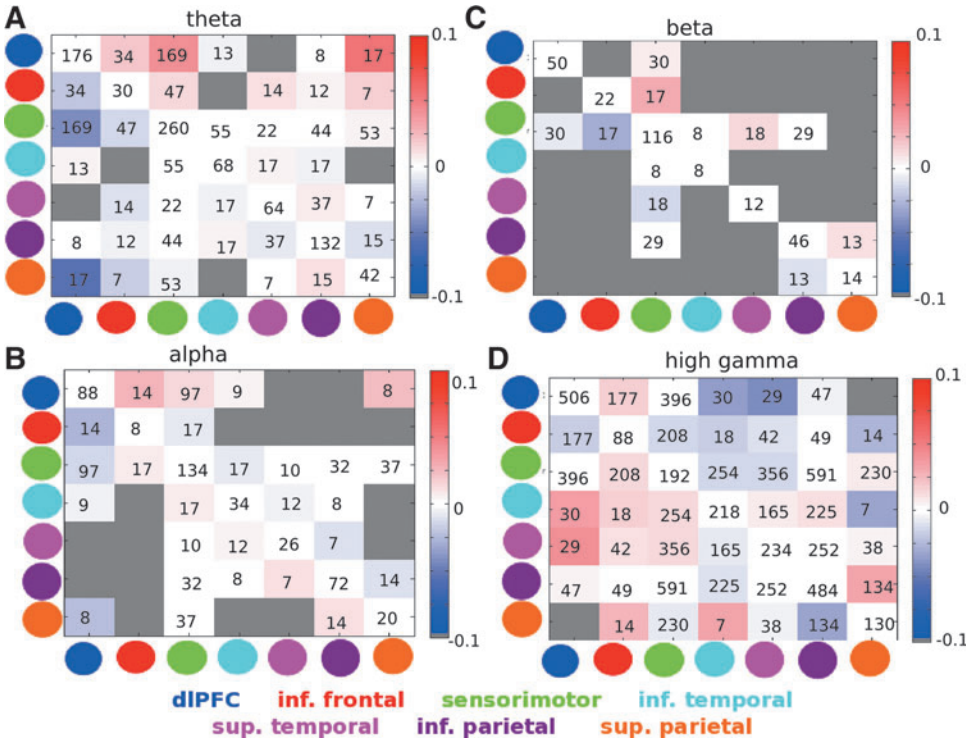

FIG. 5. Mean region-to-region PSI for **(A)** theta (4–8 Hz), **(B)** alpha (8–12 Hz), **(C)** beta (12–18 Hz), **(D)** high gamma (70–200 Hz). Note that amHG and delta are not included due to technical limitations (see the Materials and Methods section for details). Value in each box indicates number of pairs included in each comparison; comparisons with fewer than seven pairs were excluded. Rows are pseudo-causal and columns are pseudo-caused; red indicates flow (from region in row to region in column), blue indicates reverse flow (from region in column to region in row). Gray indicates pairs of regions with no significant interactions. Note the frontal-parietal, but not parietal-frontal direction of overall flow across multiple frequency bands. Plot thresholds set at ±0.1 based on the mean maximum and minimum observed PSI values. PSI, phase slope index. Color images available online at www.liebertpub.com/brain

PSI was especially strong within and between frontal regions, from frontal to parietal regions, and within and between parietal regions (Fig. 5). Interestingly, PSI is lower in all bands between temporal regions relative to all other pairs of regions, which may reflect the lack of lateral temporal involvement in known resting state networks (RSNs) (He et al., 2008). Overall, while there was widespread, multi-frequency frontal-to-parietal flow, there was virtually no parietal-to-frontal flow (Fig. 5). There appears to be a potential dlPFC-sensorimotor-parietal chain of flows in lower frequencies as this information moves anterior to posterior. This finding is notable as it demonstrates asymmetry in resting state interactions that cannot be studied with sufficient resolution and precision with fMRI due to its low temporal resolution and range of frequencies, and can only be investigated in a limited way with EEG given the far lower signal quality.

Discussion

We used phase synchrony to identify patterns of linear, band-limited electrophysiological functional connectivity in the resting state. We highlight regional phase synchrony across the full human cortical frequency spectrum within the resting state ranging from delta through HG, and including the amHG band. Our approach reveals differences between cortical regions in the frequencies with strongest phase-based connectivity, and local patterns of HG connectivity that occurred in multiple discrete near-neighbor groups. We also demonstrated that properties of resting state amHG PLVs are more similar to those of slow frequencies. This is in contrast with HG band PLVs, which show fewer significant relationships that were generally isolated to local functional boundaries, and to a lesser extent within lobes (Fig. 3 and 4). To note further is the broad connectivity of the sensorimotor region in the lower frequency ranges (e.g., delta and theta; Fig. 4). This pattern is inconsistent with the previously observed role of beta in sensorimotor regions during the resting state using MEG (Hillebrand et al., 2012) and the well-established beta idling rhythm that dominates the resting sensorimotor power spectrum (Groppe et al., 2013).

We also observed a frontal to parietal directional shift spanning multiple frequency bands of resting state phase synchrony estimates. While this study does not measure the direct influence of frontal activity on parietal activity, our PSI analyses imply that frontal regions are consistently influencing the spontaneous activities of more posterior, and specifically parietal, zones. While phase coherence in the electrophysiology of resting state has been studied (Hillebrand et al., 2012), this is the first examination of causal properties of resting state electrophysiological phase synchrony.

The range of oscillatory frequencies generated by the brain allows multiple processes to be simultaneously communicated across multiple regions. The precise type of information carried by each frequency may vary, and is dependent

on the regions involved and the distance and type of connection (Weiss and Mueller, 2012). Regions within a network, though spatially distant, must have some degree of interaction to communicate during the resting state. Phase synchrony, as examined here, is one physiological mechanism likely contributing to this level of interaction.

The PLV and non-causal interactions

Consistent with previous studies of resting state cross-frequency coupling (Florin and Baillet, 2015; Weaver et al., 2016), long distance connectivity appears to be largely dependent on low frequencies (Fig. 3A–D). Across all regions, lower frequency (alpha and slower) phase synchrony was associated to a much greater degree with both short and long-range connectivity. In contrast, with the exception of amHG band, higher frequencies (i.e., beta, HG) appeared to be almost entirely linked to local cortical regions (Fig. 3E, F).

Phase synchrony was noted between sensorimotor electrodes and electrodes from each other region across multiple frequency bands. However, the greatest magnitude effect and most consistent phase relationships noted occurred in the beta band, particularly between sensorimotor cortical electrodes and inferior temporal electrodes (Fig. 3E). This is consistent with results from a recent MEG study demonstrating a consistent pattern of resting state phase synchrony in beta and low gamma bands between sensorimotor regions and parietal and temporal regions (Hillebrand et al., 2012). This suggests that the classic sensorimotor beta ''idling'' rhythm may serve to coordinate resting state coupling of spontaneous sensorimotor activity with other functionally homogeneous neuronal assemblies spanning the lateral surface of the cortex.

We also noted frequency dependence of phase synchrony along roughly the anterior-posterior axis of the lateral neocortical surface. Generally, lowest (≤delta) frequencies had higher synchrony in frontal, especially prefrontal, regions, and the greatest anatomical extent of connectivity. In intermediate frequencies (theta through beta), preferential synchrony shifts toward posterior frontal and temporal areas and becomes sparser, while the highest frequencies (HG) have only very limited local synchrony, almost exclusively in parietal areas. Unfortunately, our ability to draw conclusions about the superior parietal region in particular is limited by the low number of electrodes located there.

This regional variation in functional connectivity patterns across frequencies, or alternatively, in preferred frequency of synchrony between pairs of regions, may be cytoarchitectural, anatomical, or functional in origin. Parietal and prefrontal association areas are cytoarchitecturally distinct from other primary cortical areas, such as sensorimotor or temporal regions (Amunts et al., 2007). These regions may support a neurophysiological environment more capable of high frequency resting state synchrony. For example, parvalbumin-containing inhibitory interneurons found in the association cortex are involved in coordinating gamma oscillations (Sohal et al., 2009). It is conceivable that the unique cytoarchitecture or anatomy in frontal and parietal association areas may enable resting state high frequency synchrony to a much greater degree. Further, the known specific cognitive and functional roles of each classic idling rhythm in the resting state, such as beta in motor, may here be reflected in the variance across cortical regions that do not equally contribute to those roles (Groppe et al., 2013).

amHG oscillations showed phase synchrony spanning much longer distances than synchrony of the HG band. The lower overall phase consistency (i.e., PLVs) between the amHG and all other bands, noted above, is likely a result of fewer total cycles available for computing phase interactions across our 8 min sampling period. Consequently, desynchronization lasting even a few cycles would represent a larger fraction of the total cycles in the amHG sample than in any of the faster frequencies, artificially lowering phase locking. Because cutoffs for statistical significance were calculated for each frequency band individually, these values are still significant despite the discrepancy with the other bands that arises from the desynchronization effect. Despite this overall drop in absolute value, the spatial patterns of connectivity indicate amHG is more analogous to low frequency bands rather than to the HG band itself. Consistent with previous studies (Keller et al., 2013; Ko et al., 2013), these results support the hypothesis that amHG cycling may act as a long-range carrier for entraining HG that is otherwise restricted to local neighborhoods. Potentially, phase coordination of the amHG band could synchronize and modulate local HG phase and amplitude activities across long-distances (Chawla et al., 1999).

The PSI and causal interactions

This study is the first to investigate causal phase relationships in the electrophysiology of resting state signals sampled directly from the cortical surface. Generally, connectivity patterns observed with PSI were consistent with PLV. PSI values appear, intuitively, quite low. Values close to zero may be due to the averaging of positive and negative numbers (indicating inconsistent flow direction), or because these networks tend to have low overall net effect on each other relative to all the inputs to a region. There are no established expected ranges for PSI in brain data. We found that net flow of spontaneous connectivity generally moves within frontal regions, most strongly from dlPFC to sensorimotor; frontal regions to parietal regions; and inferior to superior parietal. The lack of parietal-to-frontal flow cannot be attributed solely to the low number of electrode frontal-parietal electrode pairs, as unidirectional frontal-to-parietal flow was observed, as were significant PLVs between the regions. Notably, temporal regions have overall very weak causal relationships, even relative to the low PSI values overall; however, in the amHG band only, there is higher net flow from inferior to superior temporal and from inferior temporal to inferior parietal. The overall anterior-to-posterior direction of flow is consistent with findings from previous studies (Nolte et al., 2008), but is demonstrated more robustly here with great sensitivity to the high frequency signals.

The cognitive or neural mechanisms that mediate this directional flow of information are not clear, though the direction of connectivity is evident. It is likely that the same cytoarchitecture and regional anatomical differences driving PLV interactions discussed previously also contribute to causal PSI estimates, though we can derive a higher-level model of mean causal directionality from frontal and parietal regions within spontaneous resting state recordings. Several ubiquitous cortical networks, such as the default mode network, frontoparietal network, and dorsal attention network have localized hubs in frontal and parietal neocortex, likely due to regional differences between primary, secondary, and association cytoarchitecture. Hub membership may

dictate directionality as measured by PSI, potentially by regional differences in intrinsic properties of idling rhythms. Additional studies are needed to investigate regional differences in resting state phase selectivity and dominant idling power distributions.

As discussed above, the frontal-parietal flow of information may reflect known differences in the contribution of those regions to overall cognitive or anatomical variability. In this work, this need to synchronize cortical areas is indicated by PLV, and a net flow or influence is indicated by PSI.

Advantages of ECoG for resting state recordings, limitations, and future directions

An advantage of this study was our use of ECoG, rather than scalp EEG or MEG. Relative to surface-based recordings, ECoG has minimal recording noise and high spatial resolution due to avoiding scalp, bone, and fluids. This results in a relatively low influence of volume conduction and greater signal-to-noise ratio, especially in the high frequency end of the spectrum. Consequently, we were able to leverage ECoGs advantages in both very high and very low frequency ranges to investigate the phase properties of the amHG band for the first time.

Despite the inherent advantages that ECoG provides relative to surface level measurements of resting state synchrony, ECoG suffers from incomplete spatial coverage of the full cortical space. Consequently, we did not generally have spatial coverage over multiple network hubs, and were therefore not able to investigate phase dynamics across a true network structure (e.g., default mode network, dorsal attention network). This limits the number and patterns of neural populations that are available for investigation and restricts a complete interpretation of network synchrony. Additionally, samples can only be recorded from individuals presenting with intractable focal epilepsy. Due to the low number of cycles included in an 8-min period, we were unable to examine the 0.01–0.1 Hz amHG range that more closely corresponds to frequencies observed in fMRI. These limitations should be considered with these results.

This study included three adolescent (ages 10, 13, and 13) subjects. We lack sufficient sample size here to investigate development of networks in detail. Prior studies indicate that patterns of phase coherence (Thatcher et al., 2008), default mode network connectivity (Ko et al., 2011), and imaging markers of resting state functional connectivity within the areas sampled here (De Bie et al., 2012) are established well before age 10, our youngest subject. Future work will include younger subjects to specifically study early childhood developmental effects.

While PLV and PSI are both effective at capturing linear relationships inside of a single frequency band, they are not sensitive to nonlinear or cross-frequency interactions. Other methods such as bi-phase locking (Darvas et al., 2009a) and phase-amplitude coupling (Miller et al., 2012, 2014; Penny et al., 2008) have been used to examine such patterns in nonresting state data. In future, they may be used to examine other features of resting state data that the present analysis does not capture (e.g., Weaver et al., 2016).

Hillebrand et al. (2012) demonstrated a positive relationship between regional spectral power and phase synchrony. Although power effects are not the focus of the current set of analyses, their observations may have been influenced to some degree by volume conduction concerns inherent to MEG measurements. The relationship between the phase synchrony of two distinct neural populations and the amplitude or power of a region is not simple, despite the intuition that low signal power would underlie diminished population synchrony (Chawla et al., 1999; Daffertshofer and van Wijk, 2011).

Unlike Granger causality, which provides two numbers for a pair of signals (causal effect in each direction), PSI provides only one number for net flow, and does not separately estimate potential flow in the ''reverse causal'' direction (Granger, 1969; Nolte et al., 2008). However, despite these limitations, PSI has a much lower rate of false positives and also specifically is calculated from phase relationships between signals, which were of primary interest in this study.

Conclusion

Overall, our results indicate a strong consistent regional phase-related connectivity across frequency bands within the resting state. We conclude that (1) the dominant frequencies that drive phase interactions increase across the anterior-to-posterior position along the lateral surface of the cortex, (2) the phase of amHG signal follows connectivity patterns similar to slow frequency bands (delta, theta) than HG, and may act as a carrier for HG connectivity that is otherwise restricted to local neighborhoods, and (3) there appears to be an overall anterior to posterior directional flow across frequencies as measured by PSI. The observed spontaneous, consistent interactions may imply the existence of underlying oscillatory generators that drive intrinsic networks, while the variation across frequency and space hints at the differences across the brain that maybe dictated by cytoarchitectural or functional neuroanatomy. The findings contribute to understanding the variation and flow of spontaneous interactions at multiple time scales in an unprovoked fashion.

Acknowledgments

Work reported in this publication was supported by the National Science Foundation under award EEC-1028725 and by the National Institutes of Health under award NS065186. The authors thank David Caldwell, Jeneva Cronin, Kelly Collins, Jared Olson, Devapratim Sarma, and James Wu for their contributions to data collection, and David Caldwell for comments on signal processing methodology. We also thank the National Science Foundation's Center for Sensorimotor Neural Engineering at the University of Washington.

Author Disclosure Statement

No competing financial interests exist.

References

Amunts K, Schleicher A, Zilles K. 2007. Cytoarchitecture of the cerebral cortex—more than localization. Neuroimage 37: 1061–1065.

Biswal BB, et al. 2010. Toward discovery science of human brain function. Proc Natl Acad Sci U S A 107:4734–4739.

Blakely T, Miller KJ, Zanos SP, Rao RPN, Ojemann JG. 2009. Robust, long-term control of an electrocorticographic brain-computer interface with fixed parameters. Neurosurg Focus 27:E13.

Bullmore ET, Suckling J, Overmeyer S, Rabe-Hesketh S, Taylor E, Brammer MJ. 1999. Global, voxel, and cluster tests, by theory and permutation, for a difference between two groups of structural MR images of the brain. IEEE Trans Med Imaging 18:32–42.

Buzsáki G. 2004. Large-scale recording of neuronal ensembles. Nat Neurosci 7:446–451.

Cabral J, Kringelbach ML, Deco G. 2014. Exploring the network dynamics underlying brain activity during rest. Prog Neurobiol 114C:102–131.

Chawla D, Lumer ED, Friston KJ. 1999. The relationship between synchronization among neuronal populations and their mean activity levels. Neural Comput 11:1389–1411.

Conner CR, Ellmore TM, Pieters TA, DiSano MA, Tandon N. 2011. Variability of the relationship between electrophysiology and BOLD-fMRI across cortical regions in humans. J Neurosci 31:12855–12865.

Crone NE, Sinai A, Korzeniewska A. 2006. High-frequency gamma oscillations and human brain mapping with electrocorticography. Prog Brain Res 159:275–295.

Daffertshofer A, van Wijk BC. 2011. On the influence of amplitude on the connectivity between phases. Front Neuroinform 5:6.

Damoiseaux JS, et al. 2006. Consistent resting-state networks across healthy subjects. Proc Natl Acad Sci U S A 103:13848–13853.

Darvas F, Ojemann JG, Sorensen LB. 2009. Bi-phase locking—a tool for probing non-linear interaction in the human brain. Neuroimage 46:123–132.

Darvas F, Miller KJ, Rao RPN, Ojemann JG. 2009. Nonlinear phase-phase cross-frequency coupling mediates communication between distant sites in human neocortex. J Neurosci 29:426–435.

de Bie H, et al. 2012. Resting-state networks in awake five- to eight-year old children. Hum Brain Mapp 33:1189–1201.

Deckers RHR, et al. 2006. An adaptive filter for suppression of cardiac and respiratory noise in MRI time series data. Neuroimage 33:1072–1081.

Duff EP, Johnston LA, Xiong J, Fox PT, Mareels I, Egan, GF. 2008. The power of spectral density analysis for mapping endogenous BOLD signal fluctuations. Hum Brain Mapp 29:778–790.

Florin E, Baillet S. 2015. The brain's resting-state activity is shaped by synchronized cross-frequency coupling of oscillatory neural activity. Neuroimage 111:26–35.

Gohel S, Biswal BB. 2015. Functional integration between brain regions at rest occurs in mutliple-frequency bands. Brain Connect 5:23–34.

Granger CWJ. 1969. Investigating causal relations by econometric models and cross-spectral methods. Econometrica 37:424–438.

Greenblatt RE, Pflieger ME, Ossadtchi AE. 2012. Connectivity measures applied to human brain electrophysiological data. J Neurosci Methods 207:1–16.

Groppe DM, et al. 2013. Dominant frequencies of resting human brain activity as measured by the electrocorticogram. Neuroimage 79:223–233.

He BJ, Snyder AZ, Zempel JM, Smyth MD, Raichle ME. 2008. Electrophysiological correlates of the brain's intrinsic large-scale functional architecture. Proc Natl Acad Sci U S A 105:16039–16044.

Hillebrand A, Barnes GR, Bosboom JL, Berendse HW, Stam CJ. 2012. Frequency-dependent functional connectivity within resting-state networks: an atlas-based MEG beamformer solution. Neuroimage 59:3909–3921.

Hiltunen T, et al. 2014. Infra-slow EEG fluctuations are correlated with resting-state network dynamics in fMRI. J Neurosci 34:356–362.

Keller CJ, et al. 2013. Neurophysiological investigation of spontaneous correlated and anticorrelated fluctuations of the BOLD signal. J Neurosci 33:6333–6342.

Keller CJ, et al. 2014. Corticocortical evoked potentials reveal projectors and integrators in human brain networks. J Neurosci 34:9152–9163.

Kern M, Aertsen A, Schulze-Bonhage A, Ball T. 2013. Heart cycle-related effects on event-related potentials, spectral power changes, and connectivity patterns in the human ECoG. Neuroimage 81:178–190.

Ko AL, Darvas F, Poliakov A, Ojemann J, Sorensen LB. 2011. Quasi-periodic fluctuations in default mode network electrophysiology. J Neurosci 31:11728–11732.

Ko AL, Weaver KE, Hakimian S, Ojemann JG. 2013. Identifying functional networks using endogenous connectivity in gamma band electrocorticography. Brain Connect 3:491–502.

Kramer MA, Eden UT, Lepage KQ, Kolaczyk ED, Bianchi MT, Cash SS. 2011). Emergence of persistent networks in long-term intracranial EEG recordings. J Neurosci 31:15757–15767.

Lachaux JP, Rodriguez E, Martinerie J, Varela FJ. 1999. Measuring phase synchrony in brain signals. Hum Brain Mapp 8:194–208.

Mantini D, Perrucci MG, Del Gratta C, Romani GL, Corbetta M. 2007. Electrophysiological signatures of resting state networks in the human brain. Proc Natl Acad Sci U S A 104:13170–13175.

Miller KJ, Hermes D, Honey CJ, Hebb AO, Ramsey NF, Knight RT, Ojemann JG, Fetz EE. 2012. Human motor cortical activity is selectively phase-entrained on underlying rhythms. PLoS Comput Biol 8:e1002655.

Miller KJ, Honey CJ, Hermes D, Rao RP, denNijs M, Ojemann JG. 2014. Broadband changes in the cortical surface potential track activation of functionally diverse neuronal populations. Neuroimage 85:711–720.

Miller KJ, Weaver KE, Ojemann JG. 2009. Direct electrophysiological measurement of human default network areas. Proc Natl Acad Sci U S A 106:12174–12177.

Nir Y, et al. 2008. Interhemispheric correlations of slow spontaneous neuronal fluctuations revealed in human sensory cortex. Nat Neurosci 11:1100–1108.

Nolte G, et al. 2008. Robustly estimating the flow direction of information in complex physical systems. Phys Rev Lett 100:234101.

Olson JD, et al. 2016. Comparison of subdural and subgaleal recordings of cortical high-gamma activity in humans. Clin Neurophysiol 127:277–284.

Papademetris X, Jackowski M, Rajeevan N, Ojuda H, Constable RT, Staib LH. 2006. BioImage Suite: An Integrated Medical Image Analysis Suite. Section of Bioimaging Sciences, Department of Diagnostic Radiology, Yale School of Medicine. www.bioimagesuite.org Last accessed March, 2015.

Penny WD, Duzel E, Miller KJ, Ojemann JG. 2008. Testing for nested oscillation. J Neurosci Methods 174:50–61.

Sauseng P, Klimesch W. 2008. What does phase information of oscillatory brain activity tell us about cognitive processes? Neurosci Biobehav Rev 32:1001–1013.

Schalk G, McFarland DJ, Hinterberger T, Birbaumer N, Wolpaw JR. 2004. BCI2000: a general-purpose brain-computer interface (BCI) system. IEEE Trans Biomed Eng 51:1034–1043.

Schölvinck ML, Leopold DA, Brookes MJ, Khader PH. 2013. The contribution of electrophysiology to functional connectivity mapping. Neuroimage 80:297–306.

Smith SM, et al. 2009. Correspondence of the brain's functional architecture during activation and rest. Proc Natl Acad Sci U S A 106:13040–13045.

Sohal VS, Zhang F, Yizhar O, Deisseroth K. 2009. Parvalbumin neurons and gamma rhythms enhance cortical circuit performance. Nature 459:698–702.

Talairach J, Tournoux P. 1988. Co-Planar Stereotaxic Atlas of the Human Brain. New York: Thieme.

Thatcher RW, North DM, Biver CJ. 2008. Development of cortical connections as measured by EEG coherence and phase delays. Hum Brain Mapp 29:1400–1415.

Tognoli E, Kelso J. 2009. Brain coordination dynamics: True and false faces of phase synchrony and metastability. Prog Neurobiol 87:31–40.

Weaver KE, Wander JD, Ko AL, Casimo K, Grabowski TJ, Ojemann JG, Darvas F. 2016. Directional patterns of cross frequency phase and amplitude coupling within the resting state mimic patterns of fMRI functional connectivity. Neuroimage 128:238–251.

Weiss S, Mueller HM. 2012. ''Too many betas do not spoil the broth'': The role of beta brain oscillations in language processing. Front Psychol 3:201.

Address correspondence to:
Kaitlyn Casimo
University of Washington
Box 352350
Seattle, WA 98195

E-mail: kcasimo@uw.edu